3D shape identification of parallelepiped flaw by means of biaxial MFLT using neural network

ABE Masataka[1], BIWA Shiro[2], and MATSUMOTO Eiji[3]

1. Graduate School of Energy Science, Kyoto University, Kyoto, 606-8501, Japan (m.abe@ax7.ecs.kyoto-u.ac.jp)
2. Graduate School of Engineering, Kyoto University, Kyoto, 606-8501, Japan (biwa@kuaero.kyoto-u.ac.jp)
3. Graduate School of Energy Science, Kyoto University, Kyoto, 606-8501, Japan (matumoto@energy.kyoto-u.ac.jp)

Abstract: In this paper, we attempt to evaluate the three-dimensional shape of a parallelepiped flaw and identify its location, i.e. the horizontal position and the located surface, by means of biaxial Magnetic Flux Leakage Testing (MFLT), employing a Neural Network (NN). The specimen is a magnetic material (SS400) subjected to a magnetic field, and the magnetic flux in the specimen leaks near the flaw. We measure the biaxial Magnetic Flux Leakage (MFL), i.e., the tangential and the normal components of the MFL, along a line parallel to the specimen's surface. We then approximate the measured biaxial MFL distributions by means of elementary functions with a small number of coefficients. The approximation coefficients are extracted as Characteristic Quantities (CQs) of the MFL distribution. The horizontal position of the flaw along the measurement line is characterized by some of these CQs. NN is used to infer the cross section of the flaw, i.e., the width, depth, and located surface of the CQs. By repeating a similar process along several measurement lines parallel to the specimen's surface, we can identify the three-dimensional shape of the flaw, including its location. The NN, trained with several known flaws, was found to be able to evaluate the three-dimensional shape and location of a parallelepiped flaw with a high level of accuracy.

Keyword: NDT; MFLT; neural network; flaw detection; magnetic sensor

1 Introduction

Magnetic Flux Leakage Testing (MFLT) is a commonly used Non-Destructive Testing (NDT) technique for the inspection of gas or oil pipe lines, and also holds promise for structures such as rail tracks, oil storage tank floors etc.[1,2]. If a flaw exists on the surface of a ferromagnetic material located in a magnetic field, then magnetic flux leaks from the material due to variation in the magnetic properties of the region around the flaw. MFLT evaluates the flaw by means of the correlation between the flaw shape and the measured distribution of Magnetic Flux Leakage (MFL). However, the correlation is usually so complex that it is not easy for MFLT to evaluate the three-dimensional shape of a flaw quantitatively. The most important problem is signal analysis of the measured MFL [3,4]. In this paper, we use a Neural Network (NN) to obtain this correlation. NN is a recently developed data analysis tool for modeling complex relationships between inputs and outputs, which mathematically simulates the functioning of a

biological neural network [5].

In training the NN, the MFL distribution near the flaw is employed as the input, and the flaw shape as the output. In many cases, the three-dimensional flaw shapes have been calculated from planar MFL distributions [6,7]. However, this kind of method needs an extremely large training data set, for a large variety of flaw shapes. We therefore adopted a simple method in which a cross section of the flaw right below a measurement line is calculated from a one-dimensional MFL distribution on the line. The three-dimensional flaw shape can be evaluated by repeating the above procedure along several measurement lines. This method can significantly reduce the size of the data set needed for training a NN.

On the other hand, it is valid to extract a certain number of Characteristic Quantities (CQs) from the MFL for improving the learning efficiency of the NN and the accuracy of flaw reconstruction. We are proposing Regression Analysis Method (RAM) as a new method for characterizing MFL distribution [8]. In

RAM, we approximate the original MFL distribution by means of elementary functions with a small number of coefficients. The approximation coefficients are calculated as the CQs of the MFL. Since the analytical MFL distribution for a two-dimensional flaw can be expressed in elementary functions based on the magnetic dipole model [9,10], the proposed RAM should characterize the measured MFL distribution with a high level of accuracy. It is therefore possible for RAM to effectively extract CQs from the MFL distribution by means of this simple procedure.

In this paper, we attempt to evaluate a parallelepiped flaw as a notch-type defect which may have been introduced at the time of manufacture, or while it was in service. We will first introduce the elementary functions for a rectangular flaw based on the magnetic dipole model. Next, we will measure the biaxial MFL distributions of parallelepiped flaws in SS400 specimen, and calculate CQs by means of RAM. We will then construct an NN, for which the inputs are calculated CQs and the outputs are the known flaw shapes. Finally, we will evaluate the three-dimensional shapes of unknown parallelepiped flaws by means of the previously constructed NN.

2 Distribution functions of MFL

In RAM, which we proposed in the previous section, CQs are extracted from the MFL distribution by means of elementary distribution functions. In this section, we show how the elementary functions are derived from analytical expressions based on the magnetic dipole model for a rectangular flaw.
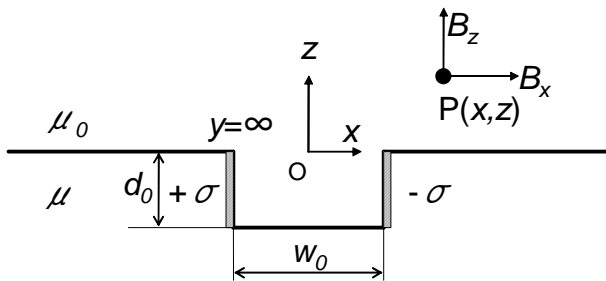

Fig.1 Rectangular flaw parameters

2.1 Rectangular flaw

The dipole model is a representative analytical expression of the MFL distribution which assumes

that positive and negative magnetic charges are uniformly distributed on each side surface of the flaw, as shown in Figure 1. We assume that the rectangular flaw is located at the origin of the coordinate axes and extends infinitely along the y axis. Therefore, the tangential and normal components of the MFL, i.e. the two-dimensional distributions of B_x and B_z, without the external magnetic field, can be expressed in the following form [9,10].

$$B_x = 2\sigma\mu_0 \left[\tan^{-1} \frac{d_0(x+w_0/2)}{(x+w_0/2)^2 + z(z+d_0)} \right.$$
$$\left. - \tan^{-1} \frac{d_0(x-w_0/2)}{(x-w_0/2)^2 + z(z+d_0)} \right] \quad (1)$$

$$B_z = \sigma\mu_0 \ln \left[\frac{(x+w_0/2)^2 + (z+d_0)^2}{(x-w_0/2)^2 + (z+d_0)^2} \frac{(x-w_0/2)^2 + z^2}{(x+w_0/2)^2 + z^2} \right] \quad (2)$$

In these equations, d_0 is the depth, w_0 the width, and σ(A/m) is the surface magnetic density. If the flaw width w_0 is sufficiently small, it can be shown that the above expressions may be approximated as

$$B_x = 2\sigma\mu_0 w_0 \left[\frac{z}{x^2 + z^2} - \frac{z+d_0}{x^2 + (z+d_0)^2} \right] \quad (3)$$

$$B_z = -2\sigma\mu_0 w_0 \left[\frac{x}{x^2 + z^2} - \frac{x}{x^2 + (z+d_0)^2} \right] \quad (4)$$

The above expressions are identical to the Forster's MFL distribution functions for a finite slot [11]. Since the horizontal position of the flaw is unknown, and in a real world situation an external magnetic field would also be present, we should modify the above expressions. We are also interested in the MFL distribution at a particular height, specifically the vertical distance of the magnetic sensor from the specimen surface. As a result, the biaxial MFL distributions at a constant vertical distance are expressed in a one-dimensional form.

$$B_x = a_x \left[\frac{b_x}{(x-d_x)^2 + b_x^2} - \frac{c_x}{(x-d_x)^2 + c_x^2} \right] + e_x \quad (5)$$

$$B_z = -a_z \left[\frac{x-d_z}{(x-d_z)^2 + b_z^2} - \frac{x-d_z}{(x-d_z)^2 + c_z^2} \right] - e_z(x-d_z) + f_z \quad (6)$$

2.2 CQs extracted by RAM

Through RAM, we approximate the MFL distributions by means of elementary functions using the least

square method, in which CQs are the coefficients contained in the functions. In Fig. 2, blank circles denote the measured biaxial MFL distribution for a front surface rectangular flaw. The solid lines in Fig. 2 show the approximated MFL distributions of Eqs. (5) and (6). The lines are properly coincident with the measured data. In Eqs. (5) and (6), coefficients d_x and d_z indicate the horizontal position of the flaw. Ideally, d_x and d_z have the same value. Coefficients e_x, e_z and f_z are the tangential and normal components of the bias magnetic flux far from the flaw. The above coefficients can be determined in the approximation process of the measured MFL distribution. Thus, in the following sections we employ the remaining six coefficients, i.e., a_x, b_x, c_x, a_z, b_z, c_z, as CQs in order to evaluate the flaw shape quantitatively. These six coefficients are considered to be CQs closely correlated with flaw shapes.

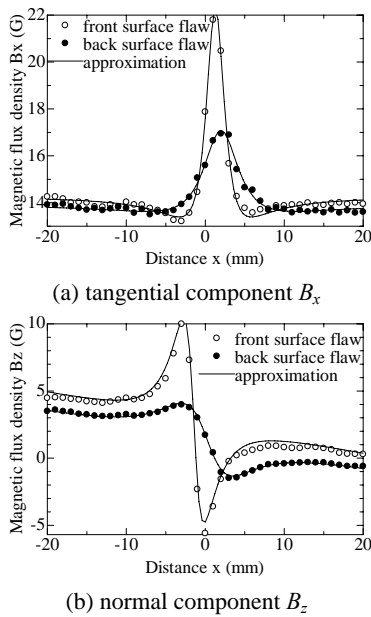(a) tangential component B_x

(b) normal component B_z

Fig.2 Approximation of biaxial MFL distributions of rectangular flaw

Meanwhile, it is known that the MFL distribution profile of a back surface flaw is similar to that of a front surface flaw. So we can therefore extract the CQs from the MFL of a back surface flaw using Eqs.(5) and (6) in the same way we do for a front surface flaw. In Fig. 2, solid circles denote the measured biaxial MFL distribution for a back surface rectangular flaw. The solid lines in Fig. 2 show the approximated MFL distributions of Eqs. (5) and (6). We can see that the lines are properly coincident with

the measured MFL data for both a back surface flaw as well as a front surface flaw.

3 MFL measurement

The specimen material is conventionally structural rolled steel SS400 whose magnetization curve is given in Fig. 3. Each specimen is 300mm length, 30mm width and 5mm thickness, and has three parallelepiped flaws at sufficiently intervals on one surface, as seen in Fig. 4. For the training of the NN we introduced 24 flaws with width w and depth d, as indicated by solid circles in Fig. 5. We measure the biaxial MFL distributions on both the front and the back surfaces with respect to the magnetic sensor, so in total we obtained 48 sets of data that were used for training the NN. For evaluating the unknown flaws we prepared 6 front and back surface flaws with width w and depth d, as indicated by blank circles in Fig. 5.
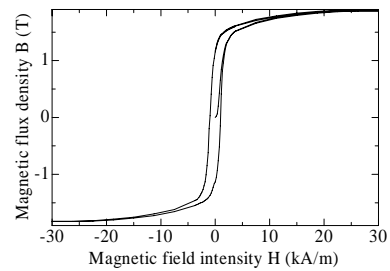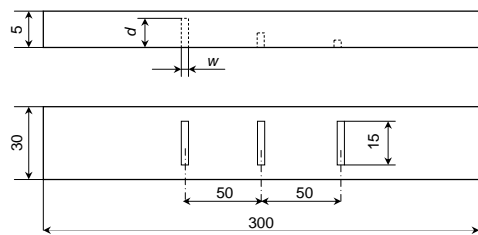

Fig.3 B-H curve of SS400
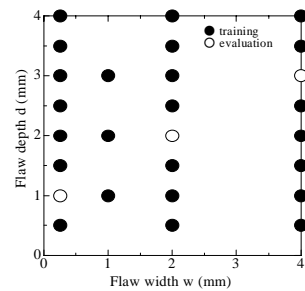

Fig.4 Specimen (SS400)

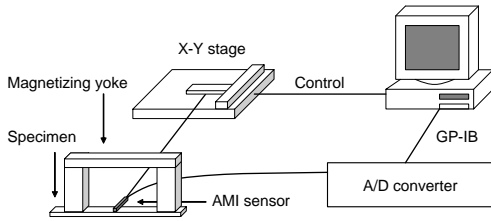Fig.5 Widths and depths of prepared parallelepiped flaws

Fig.6 Experimental system

Fig. 6 shows schematic diagram of the experimental system. The specimen was magnetized using a magnetizing yoke (HMA-1, Eishin Kagaku Co.), which has a magnetic core with a 25mm square cross section and the distance between each pole is 140mm. DC current of 0.3A we supplied to the magnetizer to induce 0.6T magnetic flux density in the cross section of the specimen, far from the flaw. The magnetic flux density was measured with an amorphous MI (Magnetic Impedance, MI-CB-1DW, AMI Co.) sensor with high spacial resolution, achieved through a 0.45mm square sensing element. Throughout the experiment, we fixed the lift-off of the sensor at 1.0mm. We measured the biaxial MFL with a pitch of 1mm along a 40mm longitudinal line centered on the flaw. We then repeated the same procedure along parallel lines at 1mm intervals throughout the 20mm wide range that includes the flaw. Thus, we measured the biaxial MFL over a 40mm×20mm area, at lattice points spaced at 1mm intervals for each one of 54 parallelepiped flaws.

4 Training of neural network

In training the NN to evaluate the shape of parallelepiped flaws, we used the 48 data sets obtained from the measurements described in the previous section. Each data set consists of 20 one-dimensional biaxial MFL distributions, meaning that we obtained a total of 960 one-dimensional biaxial MFL data points. These 960 data points include the data not only for the lines under which the flaw is present but also for those lines under which the flaw is not present. As we discussed in the previous section, we calculated all of the approximation coefficients seen in Eqs. (5) and (6) for the known flaws.

To improve the accuracy of reconstruction, we created NNs individually specified for each output. First, we would construct the NN to determine whether or not a flaw is present under each measurement line. This NN

sorts each measurement line into either the defective or non-defective category. We call this NN the classification-NN. In the classification-NN, the inputs are the six CQs a_x, b_x, c_x, a_z, b_z, c_z and the outputs are symbols d and nd which represent whether or not a flaw exists, as seen in Fig. 7. Henceforth the symbols d and nd will denote defective and non-defective, respectively. In this paper, we use the NN software, Neural Works Predict, from Neural Ware.
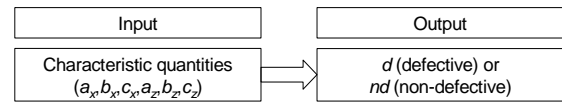

Fig.7 Structure of classification-NN

Next, we create an NN to judge the location of the flaw. We call this NN the localization-NN. For the training of this NN, we use only the data for "defective" lines, or those under which a flaw is present. In the localization-NN, the inputs are the above six CQs, and the outputs are the symbols f and b, which represent the located surface, as seen in Fig. 8. Henceforth, the symbols f and b will denote the front and back surfaces, respectively.
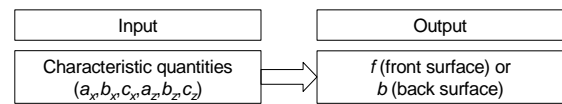

Fig.8 Structure of localization-NN

Finally, we construct a NN to identify the cross section of a flaw, i.e. the width and the depth. We call this NN the identification-NN. In training this NN, we use only the data for "defective" lines, as in the localization-NN. For the identification-NN, the inputs are the above six CQs and the outputs are the width and the depth of the flaw, as seen in Fig. 9.
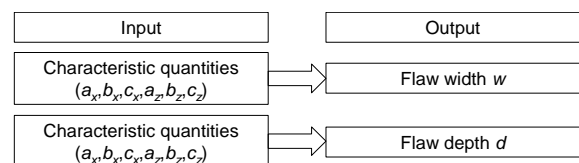

Fig.9 Structure of identification-NN

After training the NNs for each of the 48 data sets, we again estimate the known 48 flaws using the trained NNs. Table 1 shows the errors in this estimation. Fig.10 shows the estimated width and depth of each flaw. It is apparent that the estimation accuracy of

flaw depth is higher than that of flaw width. This may be due to the fact that the interval of the depth in the prepared flaws was smaller than that of the width.
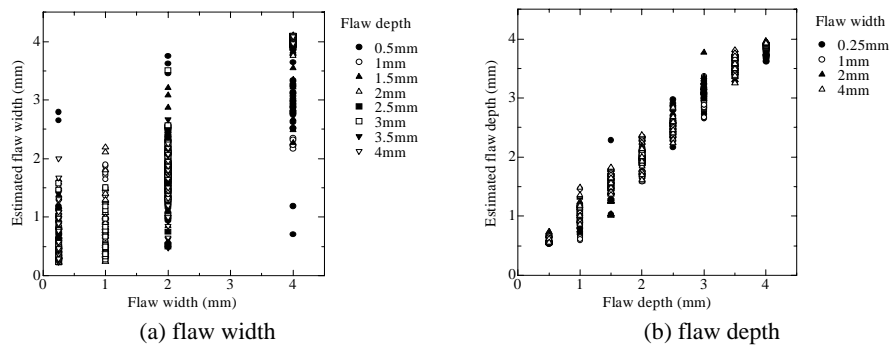

(a) flaw width   (b) flaw depth

Fig.10 Evaluation of flaws used for training NN

Table 1 Errors in evaluation of front surface flaw with 0.25mm width and 1mm depth

	Average error	Maximum error
Defective or non-defective	85.7% accuracy	
Located surface	100% accuracy	
Width	0.98mm	2.48mm
Depth	0.35mm	0.44mm

5 Evaluation of unknown flaw

For the evaluation of unknown parallelepiped flaws by means of the NNs trained as discussed above, we used the data for the 6 front and back surface flaws that we had measured as described in section 3.

We evaluated the flaws in three steps. In the first step, we used the classification-NN to estimate whether or not the data for each measurement line is defective. In the second step, we evaluated the located surface with respect to the "defective" data, that is, those data points which had been classified as defective in the first step. For this evaluation, we used the localization-NN. In the final step, we used the identification-NN to measure the depth and width of the cross section of the flaw. In this step, we evaluated only the "defective" data, as in the second step. We also assumed the horizontal position of the flaw on each measurement line to be the average value of the d_x and d_z, which is obtained at the point of extraction of CQs by means of RAM.

In Figs. 11-16, figures (a) show the flaw shapes, figures (b) show the evaluated flaw shapes, (c) and (d) show the tangential and the normal components of the measured biaxial MFL distributions. In figures (a) and (b), the graduated value denotes the depth (mm), where the negative and positive values represent the front surface and the back surface flaws, respectively. The specimen surface is assigned a value of zero. In figures (c) and (d), the graduated value denotes the magnetic flux density (G) in each direction. Tables 2-7 show the averaged error and the maximum error with respect to the 15 measurement lines which cover the opening area of each flaw. Here the error means the difference from the true value.

The accuracy of distinguishing between the defective lines and the non-defective lines by the classification-NN is between 80~95%. The accuracy of estimation of the located surface by the localization-NN is over 93%. These results show it is not likely that the flaw is overlooked or the located surface is wrongly estimated in actual inspection if the flaw passes over several measurement lines. On the other hand, the averaged errors in evaluations of the width and the depth are around 0.1 ~ 1mm. The range of above errors is in a similar order to the sensing element size or the scanning intervals. And it can be seen that the maximum error in evaluation of the width tends to be larger as the width become smaller. The averaged error and the maximum error in evaluations of the depth are around 0.3mm and 0.6mm,

respectively. Since the most important parameter for the materials diagnostics is the flaw depth, it can be said the above evaluation accuracy is enough good for practical use in material inspection.

6 Conclusion

In this paper, we attempted to evaluate the three-dimensional shape of a parallelepiped flaw in SS400, including its horizontal position and located surface by means of biaxial Magnetic Flux Leakage Testing (MFLT), using a Neural Network (NN).

(1) We adopted a simple method for evaluating the three-dimensional shape of a parallelepiped flaw, in which the three-dimensional flaw shape is obtained by integrating cross sectional evaluations of several measurement lines.

(2) We proposed a new method for extracting the Characteristic Quantities (CQs) from biaxial MFL distribution, which we call the Regression Analysis Method (RAM). We employ NN in an inverse analysis method to obtain the correlation between the above CQs and the flaw shape.

(3) We found that using biaxial MFLT with a NN, using the CQs extracted by RAM, can evaluate the three-dimensional shape and the location of the parallelepiped flaw with a high level of accuracy.

However, this proposed method can be applied only to a parallelepiped flaw. From a practical standpoint, further work is required to modify the MFL distribution functions used in RAM to represent the MFL of more arbitrarily shaped flaws.

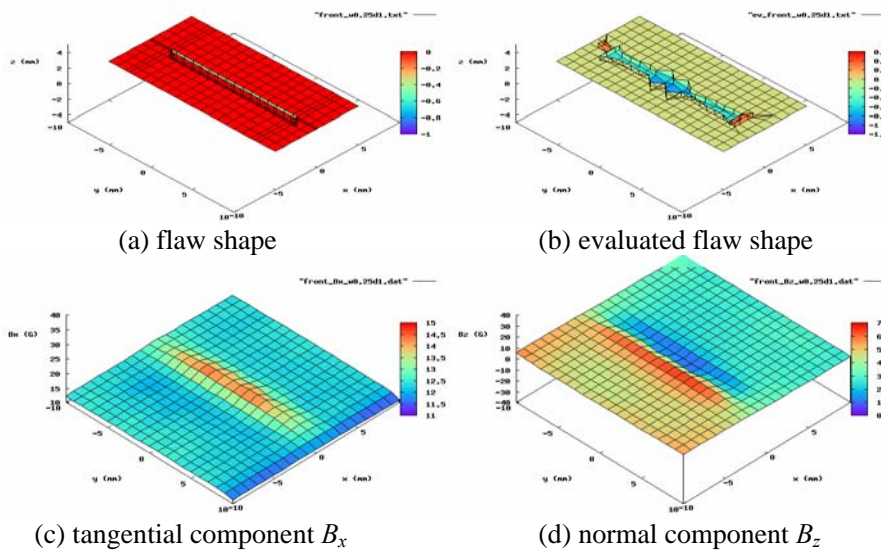| (a) flaw shape | (b) evaluated flaw shape |
| (c) tangential component B_x | (d) normal component B_z |

Fig.11 Evaluation of front surface flaw with 0.25mm width and 1mm depth

Table 2 Errors in evaluation of front surface flaw with 0.25mm width and 1mm depth

	Average error	Maximum error
Defective or non-defective	85.7% accuracy	
Located surface	100% accuracy	
Width	0.98mm	2.48mm
Depth	0.35mm	0.44mm

(a) flaw shape   (b) evaluated flaw shape

(c) tangential component B_x (d) normal component B_z
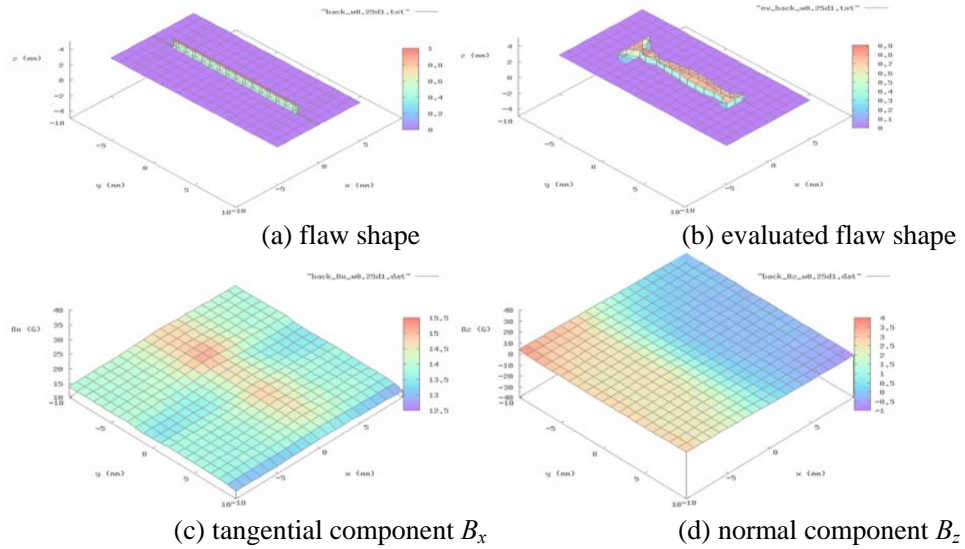
Fig.12 Evaluation of back surface flaw with 0.25mm width and 1mm depth

Table 3 Errors in evaluation of back surface flaw with 0.25mm width and 1mm depth

	Average error	Maximum error
Defective or non-defective	90.5% accuracy	
Located surface	100% accuracy	
Width	0.89mm	3.67mm
Depth	0.26mm	0.38mm

(a) flaw shape   (b) evaluated flaw shape

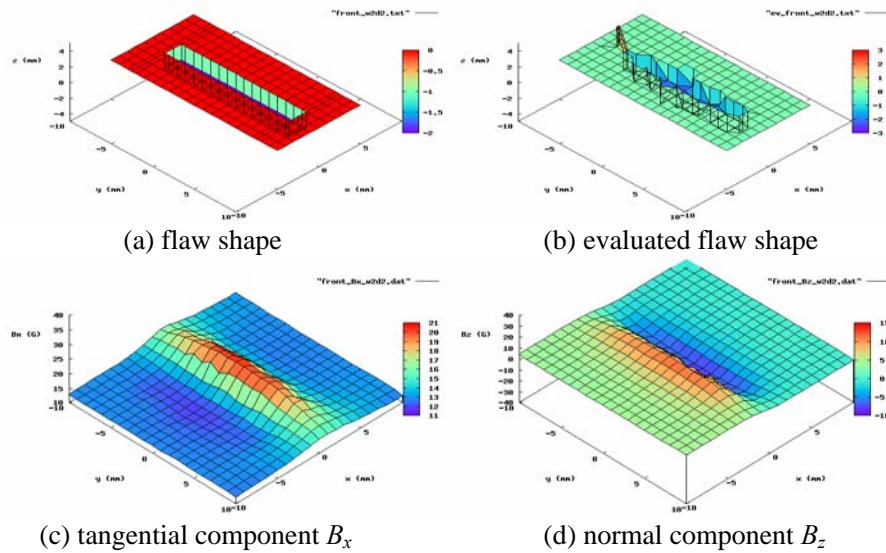(c) tangential component B_x (d) normal component B_z

Fig.13 Evaluation of front surface flaw with 2mm width and 2mm depth

Table 4 Errors in evaluation of front surface flaw with 2mm width and 2mm depth

	Average error	Maximum error
Defective or non-defective	95.2% accuracy	
Located surface	100% accuracy	
Width	0.58mm	1.99mm
Depth	0.23mm	0.64mm

(a) flaw shape

(b) evaluated flaw shape

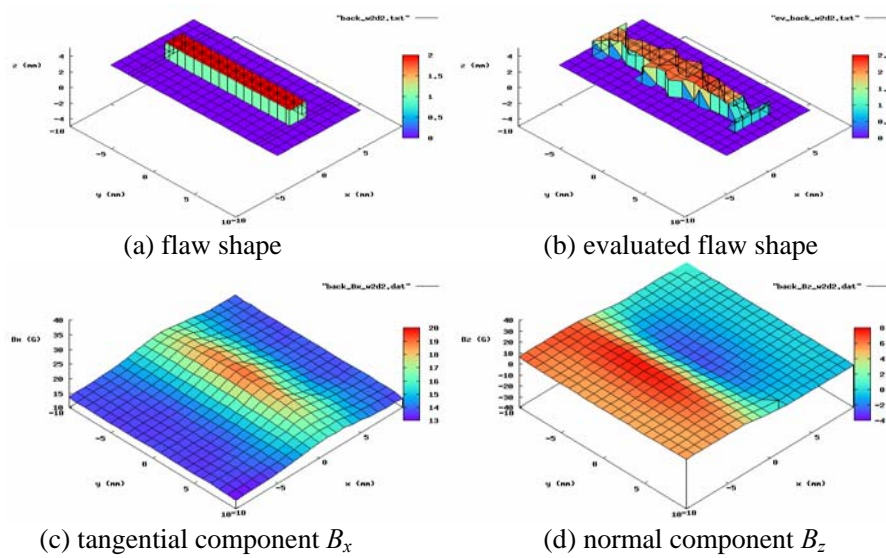(c) tangential component B_x

(d) normal component B_z

Fig.14 Evaluation of back surface flaw with 2mm width and 2mm depth

Table 5 Errors in evaluation of back surface flaw with 2mm width and 2mm depth

	Average error	Maximum error
Defective or non-defective	81.0% accuracy	
Located surface	100% accuracy	
Width	0.63mm	2.06mm
Depth	0.15mm	0.31mm

(a) flaw shape

(b) evaluated flaw shape

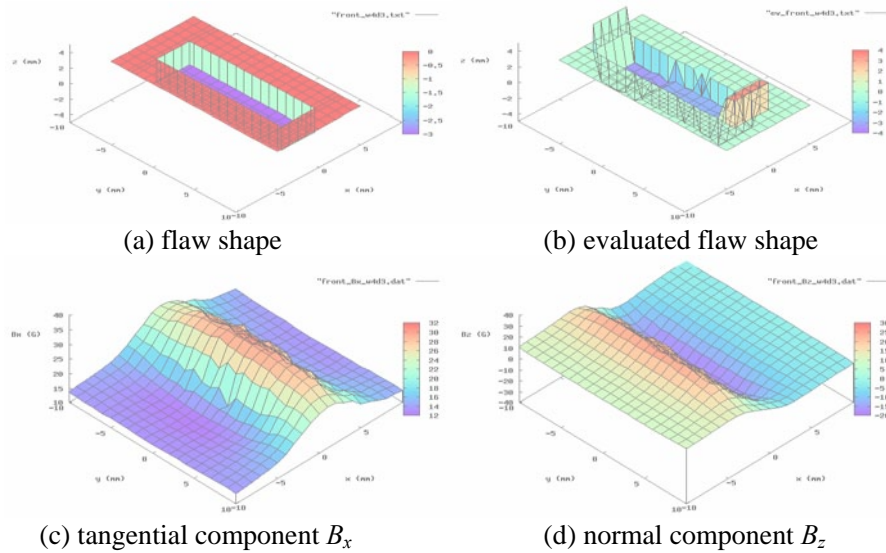(c) tangential component B_x

(d) normal component B_z

Fig.15 Evaluation of front surface flaw with 4mm width and 3mm depth

Table 6 Errors in evaluation of front surface flaw with 4mm width and 3mm depth

	Average error	Maximum error
Defective or non-defective	85.7% accuracy	
Located surface	93.3% accuracy	
Width	0.05mm	0.08mm
Depth	0.21mm	0.49mm

(a) flaw shape　　　　　　　　(b) evaluated flaw shape

(c) tangential component B_x　　　　(d) normal component B_z
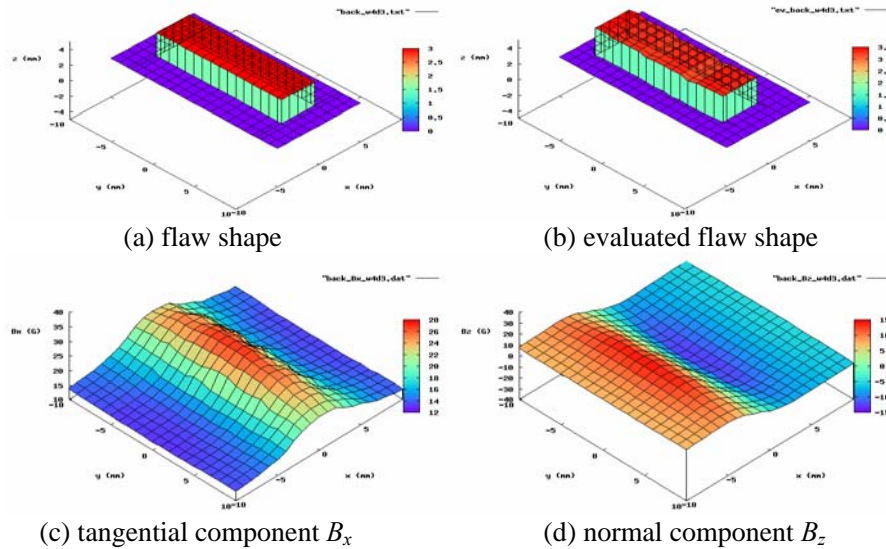
Fig.16 Evaluation of back surface flaw with 4mm width and 3mm depth

Table 7 Errors in evaluation of back surface flaw with 4mm width and 3mm depth

	Average error	Maximum error
Defective or non-defective	95.2% accuracy	
Located surface	100% accuracy	
Width	0.08mm	0.10mm
Depth	0.30mm	0.46mm

References

[1] LI, Y., WILSON, J., TIAN, G. Y.: Experiment and simulation study of 3D magnetic field sensing for magnetic flux leakage defect characterization. NDT&E International, 2007, 40: 179-184.

[2] KASAI, N., SEKINE, K., MARUYAMA, H.: Non-destructive evaluation method for far-side corrosion type flaws in oil storage tank bottom floors using the magnetic flux leakage technique. Journal of the Japan Petroleum Institute, 2003, 47 (2): 126-132.

[3] CARVALHO, A. A., REBELLO, J. M. A., SAGRILO, L. V. S., CAMERINI, C. S., MIRANDA, I. V. J.: MFL signals and artificial neural networks applied to detection and classification of pipe weld defects. NDT&E International, 2006, 39: 661-667.

[4] HAN, W., QUE, P.: 2D defect reconstruction from MFL signals by a genetic optimization algorithm. Russian Journal of Nondestructive Testing, 2005, 41 (12): 809-814.

[5] HOLLAND, J. H.: Adaptation in natural and artificial systems. Cambridge: MIT Press, 1992.

[6] HWANG, K., MANDAYAM, S., UDPA, S. S., UDPA, L., LORD, W., ATZAL, M.: Characterization of gas pipeline inspection signals using wavelet basis function neural networks. NDT&E International, 2000, 33: 531-545.

[7] JOSHI, A.: Wavelet transform and neural network based 3D defect characterization using magnetic flux leakage. International Journal of Applied Electromagnetics and Mechanics, 2008, 28: 149-153.

[8] ABE, M., BIWA, S., MATSUMOTO, E.: 3D shape evaluation of rectangular flaw by biaxial MFLT with neural network. In: Proceedings of the 20th Symposium on Electromagnetics and Dynamics, Oita: The Japan Society of Applied Electromagnetics and Mechanics, 2008, 45-50.

[9] ZATSEPIN, N. N., SHCHERBININ, V. E.: Calculation of the magnetostatic field of surface defects. I. Field topography of defect models. Defektoskopiya, 1966, 5: 50-59.

[10] SHCHERBININ, V. E., ZATSEPIN, N. N.: Calculation of the magnetostatic field of surface defects. II. Experimental verification of the principal theoretical relationships. Defektoskopiya, 1966, 5: 59-65.

[11] FORSTER, F.: Nondestructive inspection by the method of magnetic leakage fields. Theoretical and experimental foundations of the detection of surface crack of finite and infinite depth. Soviet Journal of Nondestructive Testing, 1982, 3 (11): 841-859.